Neoplasia • Vol. 7, No. 7, July 2005, pp. 658–666

www.neoplasia.com

Application of ^{23}Na MRI to Monitor Chemotherapeutic Response in RIF-1 Tumors[1]

Andriy M. Babsky, Shahryar K. Hekmatyar*, Hong Zhang*, James L. Solomon† and Navin Bansal**

Departments of *Radiology, and †Cardiology, Indiana University, Indianapolis, IN, USA

Abstract

Effects of an alkylating anticancer drug, cyclophosphamide (Cp), on ^{23}Na signal intensity (^{23}Na SI) and water apparent diffusion coefficient (ADC) were examined in subcutaneously – implanted radiation-induced fibrosarcoma (RIF-1) tumors by *in vivo* ^{23}Na and ^{1}H magnetic resonance imaging (MRI). MRI experiments were performed on untreated control (*n* = 5) and Cp-treated (*n* = 6) C3H mice, once before Cp injection (300 mg/kg) then daily for 3 days after treatment. Tumor volumes were significantly lower in treated animals 2 and 3 days posttreatment. At the same time points, MRI experiments showed an increase in both ^{23}Na SI and water ADC in treated tumors, whereas control tumors did not show any significant changes. The correlation between ^{23}Na SI and water ADC changes was dramatically increased in the Cp-treated group, suggesting that the observed increases in ^{23}Na SI and water ADC were caused by the same mechanism. Histologic sections showed decreased cell density in the regions of increased ^{23}Na and water ADC SI. Destructive chemical analysis showed that Cp treatment increased the relative extracellular space and tumor [Na^+]. We conclude that the changes in water ADC and ^{23}Na SI were largely due to an increase in extracellular space. ^{23}Na MRI and ^{1}H water ADC measurements may provide valuable noninvasive techniques for monitoring chemotherapeutic responses.

Neoplasia **7,** 658–666

Keywords: RIF-1, chemotherapy, MRI, sodium, diffusion.

Introduction

An objective and accurate quantification of early treatment response in tumors is highly desirable. Measurements of parameters such as cellular energy status [1,2], tumor lactate [3] and choline [4] levels, glycolytic rates [3,5], tissue perfusion [6], and water diffusion coefficients [7,8] by magnetic resonance (MR) techniques have been suggested as noninvasive methods for monitoring response to therapy. Commonly used anticancer therapies damage and kill tumor cells, causing an increase in interstitial space due to cell shrinkage (apoptosis) or rupture (necrosis) [9]. It has been shown using isotope techniques that the alkylating anticancer drug, cyclophosphamide (Cp), significantly increases the fraction of extracellular water [10]. Damage to tissue microvasculature may also lead to vasogenic edema, increasing the volume of extracellular water. Intracellular water may also change because of alterations in membrane permeability and ion transport processes across the cell membrane. All of these changes may alter the mobility of water in damaged tissues. The diffusion of tissue water *in vivo* can be accurately and noninvasively estimated as an apparent diffusion coefficient (ADC) by using diffusion-weighed ^{1}H nuclear magnetic resonance (NMR) [7,8,11,12]. Chenevert et al. [8] have shown that water ADC is correlated with, and highly sensitive to, changes in tumor cell density in histologic sections. Zhao et al. [7] showed a dose-dependent, reversible increase in water ADC in radiation-induced fibrosarcoma (RIF-1) tumors after Cp treatment, and the maximum water ADC increase was observed 4 days after treatment.

Monitoring and imaging tissue Na^+ by MR techniques may also be useful for assessing response to therapy because of the biologic importance of sodium. Viable cells maintain a much lower intracellular Na^+ concentration ($[Na^+]_i$) (10–30 mM) against a high extracellular Na^+ concentration ($[Na^+]_e$) (~150 mM). This transmembrane sodium gradient is maintained by the action of the Na^+/K^+ ATPase and is used to drive several vital cellular processes through the action of membrane-bound exchangers and cotransporters. For instance, intracellular pH (pH_i) is regulated, to a large extent, by a Na^+/H^+ exchanger that transports excess H^+ ions out of the cell by allowing Na^+ ions into the cell. Changes in $[Na^+]_i$ and pH_i have also been suggested to be a part of the signaling mechanism that initiates cell division and proliferation [13–15].

Abbreviations: ADC, apparent diffusion coefficient; $CoEDTA^-$, cobalt ethylenediaminetetraacetate; Cp, cyclophosphamide; DWI, diffusion-weighted images; FOV, field of view; H&E, hematoxylin and eosin; ICP, inductively coupled plasma; ip, intraperitoneal; NMR, nuclear magnetic resonance; ^{23}Na SI, ^{23}Na signal intensity; $[Na^+]_e$, extracellular sodium concentration; $[Na^+]_i$, intracellular sodium concentration; $[Na^+]_{total}$, total sodium concentration; rDW, relative dry-to-wet weight ratio; rECS, relative extracellular space; MEM, minimum essential medium; MRI, magnetic resonance imaging; MRS, magnetic resonance spectroscopy; RIF-1, radiation-induced fibrosarcoma; SNR, signal-to-noise ratio; sc, subcutaneous; T_1, longitudinal relaxation times; T_{2f} and T_{2s}, fast and slow transverse relaxation times; T_E, echo time; T_R, repetition time; WSS, weighted signal summation

Address all correspondence to: Andriy Babsky, PhD or Navin Bansal, PhD, Department of Radiology, Indiana University School of Medicine, 950 West Walnut Street, R2 E124, Indianapolis, IN 46202-5181. E-mail: ababsky@iupui.edu, nbansal@iupui.edu

[1]This research was supported, in part, by National Institutes of Health grants HL54574, CA84434, and CA94040.

Received 13 January 2005; Revised 15 March 2005; Accepted 16 March 2005.

DOI 10.1593/neo.05130

Because of its high tissue concentration, 100% natural abundance, and short T_1, ^{23}Na is the second most sensitive MR nucleus in tissues, with only ^{1}H being more sensitive. However, ^{23}Na MR signal intensity is only 1/4000 that of ^{1}H. This is largely because the water proton concentration in tissue is ~100 M, whereas the [Na^+] is only ~50 mM. In addition, the relative NMR sensitivity of ^{23}Na is 0.0925 compared to ^{1}H [16]. Thus, the low signal-to-noise ratio (SNR) of ^{23}Na, which leads to relatively long imaging times and/or poor spatial resolution, has restricted its use. Interest in ^{23}Na magnetic resonance imaging (MRI) has been revitalized with the development of more effective data acquisition schemes and hardware improvements, which now allow quantitative imaging of tissue sodium in about 15 minutes [17–19].

^{23}Na MRI signals from intracellular and extracellular compartments are isochronous because Na^+ exists in only one chemical form in tissues. The tissue [Na^+] is the volume-weighted mean of the [Na^+] in the intracellular and extracellular spaces. Thus, an increase in extracellular space as a result of therapy-induced cell loss should increase tissue [Na^+] ([Na^+]$_{tumor}$) and ^{23}Na MRI signal intensity (^{23}Na SI) because [Na^+]$_e$ is ~10 times greater than [Na^+]$_i$. The possible common mechanism for increases in water ADC and tissue ^{23}Na SI suggests that these parameters may show similar changes during or after therapy. Therapy can also alter [Na^+] because of changes in [Na^+]$_i$ as a result of altered cellular physiology and metabolism before any cellular membrane destruction. Effective therapy could increase or decrease [Na^+]$_i$ depending on the effects of therapy on cellular energy status and activity of membrane ion transport systems. Thus, ^{23}Na MRI may provide additional information than that available from water ADC measurements alone.

In the present study, we used ^{23}Na and ^{1}H MRI to examine and correlate the changes in ^{23}Na SI and water ADC in response to the chemotherapeutic drug Cp using the RIF-1 tumor model. We also investigated the mechanism of the observed changes in ^{23}Na SI and water ADC through histology and destructive chemical analysis.

Materials and Methods

Tumor Model

All animal studies were approved by the Indiana University Institutional Animal Care and Use Committee. RIF-1 tumor cells were grown in monolayers using minimum essential medium (MEM; Mediatech, Herdon, VA) supplemented with 10% fetal bovine serum, 10 mM HEPES, and 1% penicillin under a 5% CO_2 and 95% O_2 atmosphere at 37°C. The tumor cells were passaged between *in vitro* and *in vivo* states according to the protocol of Twentyman et al. [20].

Male C3H/HeN mice (Harlan, Indianapolis, IN), approximately 6 weeks old and weighing 18 to 20 g, were inoculated in the right or left flanks with a subcutaneous (sc) injection of ~2×10^6 cells in 0.10 to 0.15 ml volume of Hank's balanced salt solution. Animals were anesthetized with an intraperitoneal (ip) injection of 50 mg/kg ketamine, 5 mg/kg acepromazine, and 0.25 mg/kg atropine. The tumors were allowed to grow for 2 to 3 weeks to a volume of 1.3 to 1.6 cm^3 before performing the MRI experiments. Tumor growth was monitored by caliper measurement for planning the MRI experiments. Tumor volume was calculated from three orthogonal diameters (x, y, and z) using the formula $(\pi/6)xyz$. Ten tumor-bearing mice were treated with a single dose of Cp (300 mg/kg, ip; Sigma-Aldrich, St. Louis, MO), six of which were used for ^{1}H and ^{23}Na MRI experiments and four were used for ^{23}Na relaxation time measurements. Nine animals served as untreated controls, five of which were used for imaging experiments and the remaining animals were used for ^{23}Na relaxation time measurements. The MR experiments were performed prior to treatment with Cp and on days 1, 2, and 3 after treatment. After the 3-day posttherapy MR experiments, tumors were excised for histology or destructive chemical analysis.

In Vivo *MRI Experiments*

All MR experiments were performed on a 9.4-T, 31-cm horizontal bore system (Varian, Palo Alto, CA) equipped with a 12-cm-diameter shielded gradient set capable of up to 40 G/cm in three directions. A loop-gap resonator (inner diameter = 30 mm, depth = 25 mm) dual-tuned to 400 MHz for ^{1}H and to 106 MHz for ^{23}Na was used. The animals were anesthetized with 0.75% isoflurane delivered in medical air at 1 l/min using a mouse nose mask connected to a gas anesthesia machine (Vetland, Louisville, KY). The tumor and surrounding area were shaved to facilitate tumor measurement and coil placement. The animal was positioned on top of a custom-designed plastic cradle with the dual-tuned loop-gap resonator attached to it. The tumor was positioned inside the resonator, and the animal was held in place with tape. A detachable cylindrical phantom (6.5 mm diameter and 23 mm length) consisting of 154 mM NaCl was also placed inside the resonator to serve as a ^{23}Na MRI signal intensity and water ADC standard. Warm air was blown through the magnet bore to maintain the temperature in the space surrounding the animal at 26 to 28°C, which was monitored with a fiber optic probe (FISO Technologies, Inc., Quebec, Canada). A rectal fiber optic temperature probe was used to monitor the animal core body temperature, which remained at 36 ± 1.4°C during the MRI experiments (1–1.5 hours). The magnet was shimmed to less than 100 Hz line width at half height of the ^{1}H water signal.

^{23}Na MRI

Three-dimensional transaxial ^{23}Na MR images of the tumor were obtained using a gradient-echo imaging sequence. The following imaging parameters were used: 90 to 100 microseconds 90° excitation RF pulse, 50 milliseconds repetition time (T_R), 10 milliseconds echo time (T_E), and 64 × 32 × 8 data points over a 40 × 40 × 36 mm field of view (FOV). A relatively long T_E was used to achieve short sweep width (3700 Hz) and to optimize the SNR in ^{23}Na images. The noise in an image is directly proportional to the square root of the sweep width; thus, decreasing the

sweep width should increase the image SNR. However, decreasing the sweep width increases the acquisition time and T_E, resulting in signal loss due to T_2* relaxation. The optimum T_E and sweep width that give the maximum SNR were calculated as described by Vinitski et al. [21] from the relaxation characteristics of the tumor ^{23}Na signal and other imaging parameters used in the study. In addition, the weighted signal summation (WSS) technique was employed in the two phase-encoding directions to further improve SNR [22]. In the WSS technique, the numbers of signal transients summed at different phase-encoding steps are varied such that WSS produces similar signal conditioning effects as produced by apodization with a Gaussian function. This method of data collection increases SNR by ~50% compared to performing apodization after data collection [22]. A maximum of 128 and an average of 55 signal transients were collected for the phase-encoding steps. Total data collection time for the 3D ^{23}Na image was 14 minutes. The time domain data were zero-filled once in both phase-encoding directions (giving a 64 × 64 × 16 data matrix) and Fourier-transformed.

^{1}H MRI

Water ADC in the tumor was measured using a multislice diffusion-weighted imaging (DWI) sequence. The following imaging parameters were used: 1100 milliseconds T_R, 60 milliseconds T_E, 256 × 128 data points over a 40 × 40 FOV, 2.0 mm slice thickness, and 0.6 mm slice gap. DWI ^{1}H images were collected using four interleaved *b*-factors (b = 0, 236, 945, and 1,679 sec/mm^2). These *b*-values are similar to the values used in other publications [8,19,23]. Duration of diffusion gradient pulses was 10 milliseconds, and the delay between the gradient pulses was 40 milliseconds. The orientation of the diffusion gradients was in the read-out direction (y). Total imaging time was 19 minutes. ^{1}H images and water ADC maps were reconstructed using the Image Browser software provided by Varian. The tumor volume and average water ADC were determined over a 3D volume of interest for each temporal measurement.

^{23}Na Relaxation Time Measurements

Because the T_E used in the ^{23}Na MRI experiments was relatively long, ^{23}Na relaxation times for control and Cp-treated tumors were measured. A 10-mm-diameter surface coil was used to measure T_1 and T_2 to avoid signal contamination from normal tissues surrounding the tumor. ^{23}Na T_1 was measured using a pulse-burst saturation recovery pulse sequence consisting of 50 saturation pulses followed by an incremental delay (15 values ranging from 1 to 256 milliseconds) and a 90° observed pulse and acquisition with Cyclops phase cycling. The instrument dead time was set to 10 microseconds for all relaxation experiments. ^{23}Na T_{2f} and T_{2s} were measured using a Hahn spin-echo sequence consisting of a composite 180° pulse [24]. The T_E was varied from 0.05 to 40 milliseconds. The instrument dead time of 10 microseconds was included as a part of the T_E. One thousand twenty-four complex data points were collected over a sweep width of 3000 Hz, and either 128 or 256 transients were acquired at each relaxation delay for both T_1 and T_2 experiments. The relaxation times were computed by fitting the signal areas to both a monoexponential function and a biexponential function. The experimental conditions, including tumor volume, type of anesthesia, and drug treatment, were identical in both the ^{23}Na MRI and relaxation time experiments.

Histology

Following the last ^{1}H and ^{23}Na MRI experiments 3 days after Cp injection, the animals were sacrificed by an overdose of ketamine injected intraperitoneally. The anterior part of the tumor was marked with a permanent marker. The tumor and surrounding skin were detached from the animal body, fixed in 25% zinc–formalin solution (Anatech, Battle Creek, MI), and then embedded in paraffin. The histologic sections of the tumor were cut perpendicular to the body wall along the same plane as the MR images. Tissue sections were obtained at 5 μm thickness and stained with hematoxylin and eosin (H&E) to identify regions with different cell densities. Three histology slices, from the anterior, middle, and posterior regions of each tumor, were compared with water ADC maps and ^{23}Na MRI. During the MRI experiments, special care was taken in positioning the tumor exactly in the middle of the magnet with the help of a read-out gradient along the *z*-axis. Thus, we assume that the hitologic slices from the middle region correspond to the middle slice in the MR images. There may be a slight mismatch in orientation between the two images, but it should not affect the comparison drastically because the ^{1}H and ^{23}Na MRI slices were relatively thick (~2 mm) compared to the histologic slices (5 μm). The histologic regions with low cell density that contain relatively few intact nuclei and liquefied/caseous materials were designated as "necrotic" [25,26]. These regions can be differentiated from regions of higher cell density ("viable" regions) on lower-resolution images. Digital micrographs were obtained with a Nicon Coolpix 4500 (Nicon, Inc., Torrance, CA) and histologic slices were analyzed with Microstar IV (IMEB, Inc., Columbus, OH).

Destructive Chemical Analysis

The effects of Cp treatment on relative extracellular space (rECS) and $[Na^+]_{tumor}$ were measured by destructive chemical analysis following the last ^{23}Na relaxation time measurement 3 days after Cp injection. The animals were kept under isoflurane gas anesthesia and an 80 mM solution of cobalt ethylenediaminetetraacetate ($CoEDTA^-$; Sigma-Aldrich), an extracellular space marker, was infused through a catheter in the tail vein at 0.2 ml/hr (6 min), 0.4 ml/hr (6 min), 0.6 ml/hr (6 min), 0.8 ml/hr (6 min), and 0.5 ml/hr (60 min). As shown earlier [27,28], a similar infusion protocol allowed equilibration of CoEDTA, throughout all extracellular space in rat tissues, including the tumor. A blood sample (~0.5 ml) was withdrawn from the heart/chest area. The tumor was then quickly excised and all skin and muscles surrounding the tumor were removed. The tumor was immediately freeze-clamped using aluminum tongs precooled in liquid nitrogen, weighed, dried overnight at

60°C, and reweighed to establish the relative dry-to-wet weight ratio (rDW). The blood and tumor samples were prepared for analysis of Co^{3+} and Na^{+} by inductively coupled plasma (ICP) spectrometry using standard procedure [27]. The dried tissue samples were digested in 2 ml of concentrated nitric acid overnight in a water-heating bath held at 50°C, and blood samples were centrifuged to remove the erythrocytes from the plasma. The samples were then diluted in deionized water, and $[Na^{+}]$ and $[Co^{3+}]$ were measured by ICP at 330.232 and 228.616 nm, respectively. The rECS was determined by the equation:

$$\mathrm{rECS} = \frac{[Co^{3+}]_{tumor}}{[Co^{3+}]_{plasma}} \quad (1)$$

where $[Co^{3+}]_{tumor}$ and $[Co^{3+}]_{plasma}$ are the concentrations of Co^{3+} in the tumor and blood plasma, respectively. This method assumes that the $[Co^{3+}]$ in the extracellular space of the tumor is equal to $[Co^{3+}]_{plasma}$.

Statistical Analysis

All data are presented as the mean ± SEM. Statistical analyses of the data were performed by ANOVA (Statistica/v. 5.1 program). $P \leq .05$ was used to define statistical significance.

Results

Effect of Cp on Tumor Growth

The mean tumor volumes of control and treated mice measured from ^{1}H MRI are shown in Figure 1*A*. Before treatment, both groups had similar tumor volumes (1.3 ± 0.2 cm^3 for control group, 1.7 ± 0.2 cm^3 for treated group; $P = .18$). In Cp-treated animals, the mean tumor volume decreased to 1.3 ± 0.2 cm^3 ($P \leq .05$ *vs* pretreatment) on day 2 and to 1.1 ± 0.2 cm^3 ($P \leq .05$ *vs* pretreatment) on day 3 after treatment. The mean tumor volume in control animals (1.7 ± 0.2 cm^3) was greater ($P \leq .05$) than the baseline volume 3 days after treatment. The mean tumor volume in treated animals was significantly lower than in control animals 3 days after treatment ($P \leq .01$).

ADC of Water

The mean water ADC values in control and treated tumors prior to and after Cp injection are shown in Figure 1*B*. Water ADC was similar in control and treated groups (4.4 ± 0.2 × 10^{-4} and 4.9 ± 0.2 × 10^{-4} mm^2/sec, respectively) prior to treatment. In the control group, the mean water ADC did not change significantly over the 3 days, whereas in the treated group, water ADC increased significantly 2 and 3 days after Cp injection (5.8 ± 0.3 × 10^{-4} and 7.3 ± 0.4 × 10^{-4} mm^2/sec, respectively) compared to baseline ($P \leq .05$) and control tumors ($P \leq .01$) for both time points.

Examples of a pixel-by-pixel water ADC map for a control tumor and a treated tumor before and 1, 2, and 3 days after Cp injection are shown in Figure 2. The water ADC

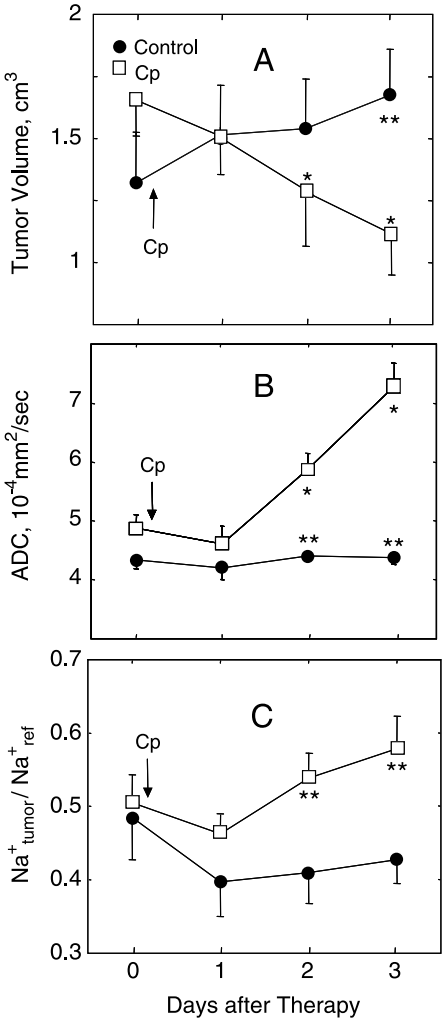

Figure 1. *Effects of Cp therapy (300 mg/kg, ip) on tumor volume (A), water ADC (B), and ^{23}Na SI from the tumor relative to the reference (Na^{+}_{tumor}/Na^{+}_{ref}) (C) in sc implanted RIF-1 tumors. Tumor volumes were measured from ^{1}H MRI. Water ADC and relative ^{23}Na SI changes are the mean from the whole tumor. Cp treatment caused a significant decrease in tumor volume and significant increases in water ADC and ^{23}Na SI 2 and 3 days posttherapy. Significance: P ≤ .05 (*– versus before treatment), P ≤ .01 (** – control versus Cp-treated). Data are presented as mean ± SEM.*

values before Cp treatment (day 0) were 4.9 × 10^{-4} and 5.4 × 10^{-4} mm^2/sec in the control and treated tumors, respectively. After Cp injection, water ADC increased progressively to 5.9 × 10^{-4} , 6.5 × 10^{-4} , and 7.6 × 10^{-4} mm^2/sec on days 1, 2, and 3, respectively. The water ADC increase was observed not only in tumor regions with low cell density (bright region in the lower right quadrant of the tumor in Figure 2) but throughout the whole tumor. In the untreated tumor, water ADC decreased slightly and was 4.5 × 10^{-4} mm^2/sec on day 3.

^{23}Na MRI and Magnetic Resonance Spectroscopy (MRS)

Figure 2 also shows ^{23}Na MR images of the same control and treated tumors before and 1, 2, and 3 days after Cp injection. Similar to the water ADC maps, ^{23}Na MRI showed heterogeneous signal intensity in both tumors, reflecting

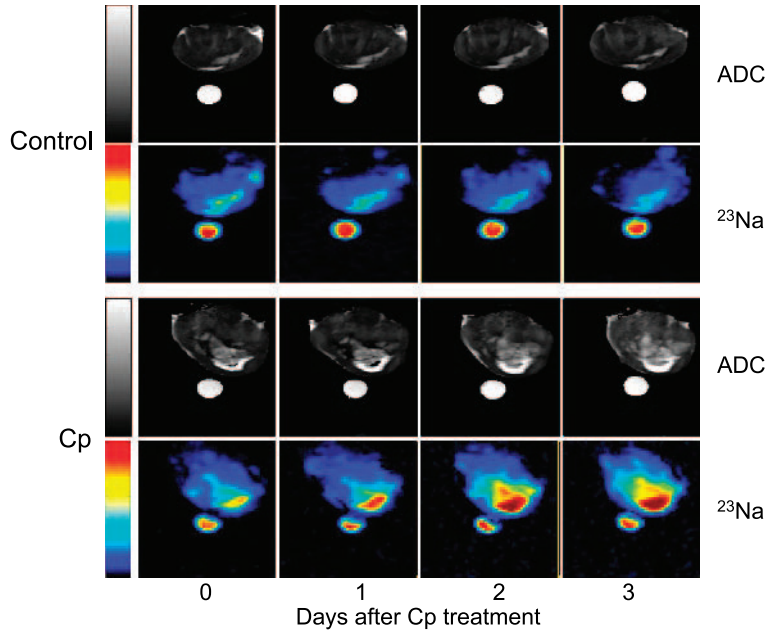

Figure 2. *Water ADC maps and ^{23}Na MR images of representative control and Cp-treated RIF-1 tumors before and 1, 2, and 3 days after Cp treatment. Water ADC and ^{23}Na signal intensity increased with time after Cp treatment. A vial filled with a 154-mM NaCl solution was placed near the tumor as a reference.*

the inherent heterogeneity in the tumor microenvironment. In the control tumor, the ^{23}Na signal was relatively stable and even slightly decreased by day 3. However, in the treated tumor, the ^{23}Na SI increased steadily (44% by day 3 after Cp injection). The most dramatic increase in ^{23}Na signal was observed in the region with low cell density, but an increase in signal intensity was detected throughout the tumor. Similar increases in ^{23}Na SI were observed in all the treated tumors.

The changes in tumor ^{23}Na SI with respect to the reference signal intensity for control and treated groups prior to and after Cp injection are shown in Figure 1*C*. The mean of tumor to reference ^{23}Na SI ratio was similar for the control and Cp-treated groups at baseline: 0.48 ± 0.06 and 0.51 ± 0.04, respectively. The ratio did not change significantly for the control group. The treated group showed a progressive increase in tumor ^{23}Na SI. The tumor to reference ^{23}Na SI ratio was 0.54 ± 0.03 on day 2 and 0.58 ± 0.04 on day 3 after Cp injection ($P \leq .05$ compared to the same time points for control).

The values of T_1, T_{2s}, and T_{2f}, and the relative contribution of T_{2s} to the observed ^{23}Na signal for control and Cp-treated tumors are listed in Table 1. There were no significant differences in the relaxation times or the relative contribution of the fast and slow relaxation components between control and treated tumors at any time point ($P \geq .1$). These relaxation parameters were measured using a separate group of animals than that used in the MRI experiments for two reasons. First, the imaging experiments took over an hour and we did not want to keep the animals under anesthesia and strained conditions any longer. Second, a surface coil was used for the relaxation time measurements to avoid contamination from healthy tissues near the tumor. The experimental conditions, including tumor volume, type of anesthesia, and drug treatment, were identical in both the ^{23}Na MRI and relaxation time experiments.

Correlation between Water ADC and ^{23}Na MRI

Spatial correlation between water ADC and ^{23}Na SI for the control and treated tumors is apparent in the images shown in Figure 2. The regions with high water ADC are also hyperintense in ^{23}Na MRI. Figure 3 shows a plot of mean water ADC and mean ^{23}Na SI for control and treated tumors. Each data point represents all the tumors at a specific day. Although the correlation between water ADC and $[Na^+]_{tumor}$

Table 1. Experimental Relaxation Times of ^{23}Na Signal from Control and Cp-Treated Tumors Before and After Therapy.

	Day 0	Day 1	Day 2	Day 3
T_1 (msec)				
Control	43.1 ± 3.6	40.6 ± 1.4	42.8 ± 3.5	43.6 ± 1.1
Cp-treated	42.0 ± 1.8	38.9 ± 0.4	43.1 ± 0.7	44.7 ± 1.7
T_{2s} (msec)				
Control	22.7 ± 0.4	22.5 ± 0.6	22.0 ± 1.1	21.1 ± 0.6
Cp-treated	25.4 ± 1.7	21.6 ± 1.1	24.8 ± 0.5	26.1 ± 0.6
T_{2f} (msec)				
Control	3.1 ± 0.2	3.2 ± 0.3	2.8 ± 0.1	2.8 ± 0.1
Cp-treated	3.7 ± 0.7	2.8 ± 0.2	3.5 ± 0.3	3.3 ± 0.2
Relative contribution from T_{2f}				
Control	0.52 ± 0.01	0.50 ± 0.01	0.53 ± 0.01	0.56 ± 0.03
Cp-treated	0.43 ± 0.05	0.47 ± 0.02	0.49 ± 0.01	0.48 ± 0.01

Values are reported as mean ± SEM (n = 4 for each group). No significant differences were found between control and Cp-treated tumors at any time point studied.

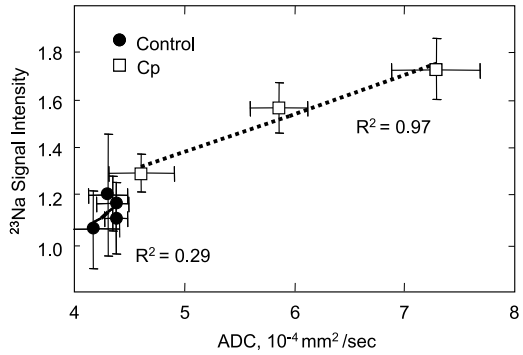

Figure 3. *Correlation between mean water ADC and ^{23}Na SI in untreated (●) and Cp-treated (□) RIF-1 tumors. Each data point represents all the tumors at a specific day. The R^2 coefficient for Cp-treated tumors was more than three times higher than for the untreated tumors.*

was poor in the control tumors, the correlation was significant (R^2 = 0.97) in Cp-treated tumors.

Histology

H&E–stained sections (low and high resolution, 20×) of a control and a Cp-treated tumor and the corresponding water ADC maps and ^{23}Na images are shown in Figure 4. MRI maps and histologic segments have a slice thickness of 2 mm and 5 μm, respectively. Viable tissue is visible in the low-resolution histologic segments as the darker purple color, and necrotic areas are visible as the brighter pink areas. There is reasonable agreement between the MR images and the histologic sections in both tumors. For example, in the Cp-treated tumor, the region with the highest Na^+ signal intensity corresponded to the histologic region with the lowest cell density (histologic section D), and the region with the lowest Na^+ signal intensity corresponded to the most viable histologic section (C). Comparison of histologic sections of control and Cp-treated tumors shows that both high and low cell density regions of treated tumors (C and D) contain fewer cells than control tumors (A and B). The necrotic regions with low cell density of both control and Cp-treated tumors also contained high extracellular collagen, a characteristic of fibrosarcoma.

Destructive Chemical Analysis

The ICP data for tissue compartmentalization and Na^+ content for control and Cp-treated tumors 3 days after treatment are shown in Table 2. In Cp-treated tumors, rDW was significantly lower ($P \leq .05$) and rECS was significantly higher ($P \leq .05$) compared to the untreated tumors. The $[Na^+]_{tumor}$ was 29.4% higher in Cp-treated tumors than in control tumors (58 ± 10 and 45 ± 7 mM, respectively; $P \leq .05$).

Discussion

In this study, we examined the effects of Cp treatment on ^{23}Na MRI as a noninvasive marker of tumor response to cancer chemotherapy and compared these Na^+ signal changes with water ADC measured by diffusion-weighted ^{1}H MRI. The Cp injection caused a significant reduction in tumor volume 2 and 3 days posttreatment. Poptani et al. [5] and Zhao et al. [7] have shown similar changes in RIF-1 tumor volumes after Cp treatment. Cp itself is a prodrug, which is oxidized in the liver to 4-hydroxycyclophosphamide and subsequently converted to nitrogen mustard and other metabolites. In RIF-1 tumors, Cp metabolites do not directly disrupt cell metabolism, but rather these metabolites alkylate DNA and proteins. It has been shown [29,30] that for RIF-1 and other animal tumors, Cp causes cell death by stimulating apoptosis, as evidenced by the induction of plasma membrane blebbing, DNA fragmentation, and cleavage of the caspase 3 and caspase 7 substrate poly(ADP-ribose) polymerase. These genetic and cellular transformations lead to some metabolic effects of Cp, such as a decrease in mitotic activity [5,31], an increase in water diffusion, and an

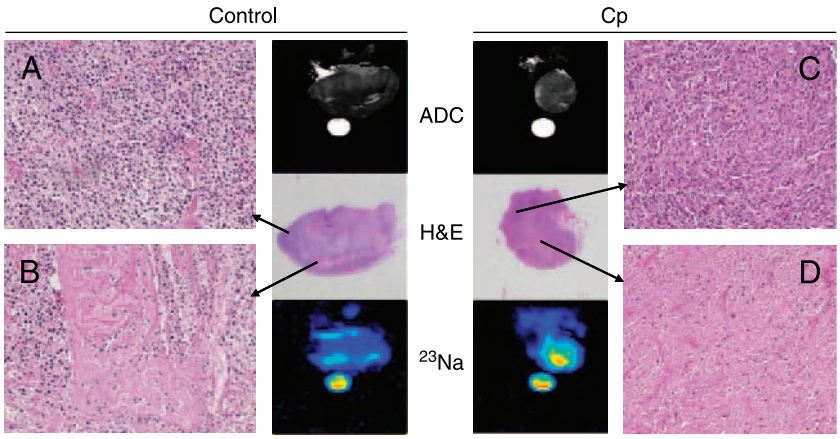

Figure 4. *H&E–stained histologic slices, water ADC maps, and ^{23}Na MRI images of representative control and Cp-treated RIF-1 tumors 3 days after treatment. Histologic and MRI slices from the middle part of the tumors are presented. Arrows point to the regions identified as "viable" (A and C) and "necrotic" (B and D) in both tumors. These regions are presented as high-resolution (original magnification, ×20) histologic images. The regions of tumors with higher ^{23}Na signal and water ADC mostly correspond to the histologic regions with fewer cells.*

Table 2. Tissue Compartmentalization and Na^+ Content of Control and Cp-Treated RIF-1 Tumors 3 Days After Therapy as Measured by Destructive Chemical Analysis.

	rDW	rECS	$[Na^+]_{tumor}$ (mM)
Control	0.21 ± 0.01	0.26 ± 0.04	45 ± 7
Cp-treated	0.16 ± 0.01*	0.46 ± 0.08*	58 ± 10*

Values are reported as mean ± SEM (n = 7 for control and n = 5 for Cp-treated group).
*Significance: $P \leq .05$ (control vs. Cp-treated).

increase in aerobic metabolism that decreases the glycolytic rate in RIF-1 cells [5].

We have shown that treatment of RIF-1 tumors with 300 mg/kg Cp significantly increased water ADC 2 and 3 days posttreatment. Braunschweiger [10] and Makin [30] have shown that Cp-induced changes in tissue microvasculature and apoptotic/necrotic damage of tumor cells lead to large reductions in cell volume and increases in the volume of extracellular water. These changes may increase the mobility of water in the damaged tissue and lead to an increase in water ADC in Cp-treated tumors, as we have shown. Our ICP and histologic results also support this hypothesis. The ICP data show a significant increase in rECS, whereas the histologic data show a decrease in the number of cells and an increase in extracellular space (Figure 3). It has been shown previously that the increase in water ADC correlates with both the increase in tumor necrotic fraction in RIF-1 tumors [25] and the decrease in tumor cell density in 9L glioma [8].

The *b*-values used in this work are similar to the values used in other publications [8,19,23]. We did not detect any nonexponential behavior with these *b*-values. Such behavior could be detected by using higher *b*-values and a larger number of data points. However, we did not attempt this because it would require long data collection times, especially at high *b*-values where SNR is low. We were simply interested in using water ADC as a therapy response parameter.

The increase in extracellular space following therapy can cause not only an increase in water ADC but also an increase in $[Na^+]_{tumor}$, as $[Na^+]_e$ is 10 to 15 times higher than $[Na^+]_i$. We found that, on average, both ^{23}Na SI and water ADC increased throughout the tumor after Cp treatment. The increase in ^{23}Na SI after chemotherapy could be because of an increase in $[Na^+]_{tumor}$ or a change in ^{23}Na relaxation times. Our data showed that Cp treatment or untreated growth of RIF-1 tumors did not significantly change the T_1, T_{2s}, and T_{2f} values, or the relative contributions of T_{2s} and T_{2f} (Table 1). These results suggest that the observed increase in ^{23}Na MRI signal intensity after Cp treatment was due to increases in $[Na^+]_{tumor}$ caused by Cp treatment. Our ICP data confirmed that in Cp-treated tumors, $[Na^+]_{tumor}$ is significantly increased 3 days after treatment (45 ± 7 mM, control; 58 ± 10 mM, Cp-treated) (Table 2). The value of the Cp-induced increase in $[Na^+]_{tumor}$ was comparable for both MRI (36.8%) and ICP (29.4%) methods.

Although the extracellular space increases after therapy, we believe that $[Na^+]_e$ remains constant. $[Na^+]_e$ can be maintained constantly by the transport of Na^+ from the vascular and/or interstitial space of the nearby uncompromised tissue even in hypoxic or necrotic regions. Moreover, previous ^{1}H MRI studies show that tumor perfusion is increased after therapy [5]. Thus, transport of Na^+ from the vascular space can maintain $[Na^+]_e$, and an increase in extracellular space results in increased $[Na^+]_{tumor}$ after therapy.

There was a good correlation between ^{23}Na SI and water ADC in the Cp-treated tumors (Figure 3). One possible reason for this effect may be that $[Na^+]_{tumor}$ increases with increased extracellular space because of cells lost through apoptosis and/or necrosis. Schepkin et al. [19] also showed that a large increase in ^{23}Na MRI signal intensity occurred 7 to 9 days following treatment with 1,3-bis (2-chlorethyl)-1-nitrosourea (BCNU; another chemotherapeutic alkylating agent), which correlated to the period of the greatest chemotherapy-induced cellular necrosis based on water ADC changes and histopathology.

Changes in $[Na^+]_{tumor}$ and water ADC may be related, but ^{23}Na images may provide more functional information because therapy can also alter $[Na^+]_i$, which depends on the cellular energy status and activity of ion transport processes. Many reports show that radiotherapy and most chemotherapies (including treatment of RIF-1 tumors with Cp) cause increased ATP levels and decreased P_i in experimental tumors [1,32,33]. This effect is thought to be a result of increased perfusion and oxygenation of the tumor [3,5,34]. The improved cellular energy status should aid in maintaining low $[Na^+]_i$ because of the high activity of the Na^+ /K^+ ATPase. However, a decrease in $[Na^+]_i$ following effective therapy may not be a general phenomenon. An ischemia-like response of tumors to therapy (decreased ATP level) and/or partial destruction of the cellular membrane or membrane-embedded proteins can produce an increase in $[Na^+]_i$. For example, Ben-Yoseph and Ross [35] demonstrated that treatment of sc implanted 9L glioma with polyethylene glycol–stabilized glucose oxidase results in a 96% reduction in the ATP/P_i and a 0.72-U decline in pH_i. In this case, $[Na^+]_i$ should increase. Thus, because of the sensitivity of ^{23}Na MRI to cellular function, it may provide additional information than that available from water ADC measurements alone.

Differences in tumor model and treatment can play important roles in tumor Na^+ response. In contrast to Schepkin et al. [19] and the results presented here, Winter et al. [27] show that BCNU therapy of subcutaneously implanted 9L glioma results in decreased SQ and TQF ^{23}Na SI compared to untreated control tumors. This difference in therapy response could be because of differences in rECS changes in the different tumor models. Winter et al. [27] did not observe any difference in rECS between treated and untreated tumors but showed improved cellular energetics and increased pH_i in sc implanted 9L glioma after BCNU therapy. These metabolic changes could decrease intracellular and total tissue Na^+. We have performed some initial ^{23}Na MRI and water ADC measurements on subcutaneously implanted 9L glioma with BCNU therapy. Our preliminary data suggest that both tissue

Na^+ and water ADC are lower in BCNU-treated tumors compared to untreated controls.

Usually both water ADC maps and ^{23}Na images had some verifiable heterogeneity in subcutaneously implanted RIF-1 tumors. In some regions, when ^{23}Na SI was high, water ADC was not dramatically increased. A possible reason for this discrepancy may be that ^{23}Na SI can also increase as a result of increase in $[Na^+]_i$. Movement of Na^+ and water into the cells can cause a decrease in water ADC because of a high macromolecule concentration inside the cells. An increase in extracellular space increases both water ADC and $[Na^+]_{tumor}$, whereas cytotoxic edema decreases water ADC but increases $[Na^+]_{tumor}$. Thus, a combination of both increased extracellular space and cytotoxic edema can cause the observed discrepancy between water ADC and ^{23}Na SI.

Conclusions

In vivo MRI experiments showed that both ^{23}Na SI and water ADC increase 2 days after chemotherapy of subcutaneously implanted RIF-1 tumors with Cp. These effects were largely due to an increase in extracellular space as shown by histology and destructive chemical analysis. The increase in ^{23}Na MRI signal intensity after Cp treatment observed in this study may prove useful for detecting early therapy response and may support the mechanism for water ADC changes.

Acknowledgements

The authors thank Paige Hopewell, Rebecca Kerkhoff, and Samuel G. Jennings for valuable comments and assistance in the preparation of the manuscript; and Yonghua Xu and Mandar Jagtap for help with analysis of histologic slices.

References

[1] Li SJ, Wehrle JP, Rajan SS, Steen RG, Glickson JD, and Hilton J (1988). Response of radiation-induced fibrosarcoma-1 in mice to cyclophosphamide monitored by *in vivo* ^{31}P nuclear magnetic resonance spectroscopy. *Cancer Res* **48,** 4736–4742.

[2] Street JC, Mahmood U, Matei C, and Koutcher JA (1995). *In vivo* and *in vitro* studies of cyclophosphamide chemotherapy in a mouse mammary carcinoma by ^{31}P NMR spectroscopy. *NMR Biomed* **8,** 149–158.

[3] Poptani H, Bansal N, Jenkins WT, Blessington D, Mancuso A, Nelson DS, Feldman M, Delikatny EJ, Chance B, and Glickson JD (2003). Cyclophosphamide treatment modifies tumor oxygenation and glycolytic rates of RIF-1 tumors: ^{13}C magnetic resonance spectroscopy, Eppendorf electrode, and redox scanning. *Cancer Res* **63,** 8813–8820.

[4] Poptani H, Pickup S, Delikatny EJ, Magnitsky S, Mancuso A, Nelson DS, and Glickson JD (2004). Increased diffusion coefficient with decreased choline in response to cyclophosphamide therapy of RIF-1 tumors. *Proc Int Soc Magn Reson Med* **11,** 2035.

[5] Poptani H, Bansal N, Graham RA, Mancuso A, Nelson DS, and Glickson JD (2003). Detecting early response to cyclophosphamide treatment of RIF-1 tumors using selective multiple quantum spectroscopy (SelMQC) and dynamic contrast enhanced imaging. *NMR Biomed* **16,** 102–111.

[6] Robinson SP, McIntyre DJ, Checkley D, Tessier JJ, Howe FA, Griffiths JR, Ashton SE, Ryan AJ, Blakey DC, and Waterton JC (2003). Tumour dose response to the antivascular agent ZD6126 assessed by magnetic resonance imaging. *Br J Cancer* **88,** 1592–1597.

[7] Zhao M, Pipe JG, Bonnett J, and Evelhoch JL (1996). Early detection of treatment response by diffusion-weighted ^{1}H-NMR spectroscopy in a murine tumour *in vivo*. *Br J Cancer* **73,** 61–64.

[8] Chenevert TL, Stegman LD, Taylor JM, Robertson PL, Greenberg HS, Rehemtulla A, and Ross BD (2000). Diffusion magnetic resonance imaging: an early surrogate marker of therapeutic efficacy in brain tumors. *J Natl Cancer Inst* **92,** 2029–2036.

[9] Latour LL, Svoboda K, Mitra PP, and Sotak CH (1994). Time-dependent diffusion of water in a biological model system. *Proc Natl Acad Sci USA* **91,** 1229–1233.

[10] Braunschweiger PG (1988). Effect of cyclophosphamide on the pathophysiology of RIF-1 solid tumors. *Cancer Res* **48,** 4206–4210.

[11] Stegman LD, Rehemtulla A, Hamstra DA, Rice DJ, Jonas SJ, Stout KL, Chenevert TL, and Ross BD (2000). Diffusion MRI detects early events in the response of a glioma model to the yeast cytosine deaminase gene therapy strategy. *Gene Ther* **7,** 1005–1010.

[12] Ross BD, Chenevert TL, and Rehemtulla A (2002). Magnetic resonance imaging in cancer research. *Eur J Cancer* **38,** 2147–2156.

[13] Cameron IL, Smith NK, Pool TB, and Sparks RL (1980). Intracellular concentration of sodium and other elements as related to mitogenesis and oncogenesis *in vivo*. *Cancer Res* **40,** 1493–1500.

[14] Koch KS and Leffert HL (1979). Increased sodium ion influx is necessary to initiate rat hepatocyte proliferation. *Cell* **18,** 153–163.

[15] Kline RP, Wu EX, Petrylak DP, Szabolcs M, Alderson PO, Weisfeldt ML, Cannon P, and Katz J (2000). Rapid *in vivo* monitoring of chemotherapeutic response using weighted sodium magnetic resonance imaging. *Clin Cancer Res* **6,** 2146–2156.

[16] Seshan V and Bansal N (1996). *In vivo* ^{31}P and ^{23}Na NMR spectroscopy and imaging. NMR Spectroscopy Techniques. In Bruch MD, Ed. Marcel Dekker, New York, NY. pp. 557–607.

[17] Ouwerkerk R, Bleich KB, Gillen JS, Pomper MG, and Bottomley PA (2003). Tissue sodium concentration in human brain tumors as measured with ^{23}Na MR imaging. *Radiology* **227,** 529–537.

[18] Thulborn KR, Davis D, Adams H, Gindin T, and Zhou J (1999). Quantitative tissue sodium concentration mapping of the growth of focal cerebral tumors with sodium magnetic resonance imaging. *Magn Reson Med* **41,** 351–359.

[19] Schepkin VD, Ross BD, Chenevert TL, Rehemtulla A, Sharma S, Kumar M, and Stojanovska J (2004). Sodium magnetic resonance imaging of chemotherapeutic response in a rat glioma. *Magn Reson Med* **53,** 85–92.

[20] Twentyman PR, Brown JM, Gray JW, Franko AJ, Scoles MA, and Kallman RF (1980). A new mouse tumor model system (RIF-1) for comparison of end-point studies. *J Natl Cancer Inst* **64,** 595–604.

[21] Vinitski S, Griffey R, Fuka M, Matwiyoff N, and Prost R (1987). Effect of the sampling rate on magnetic resonance imaging. *Magn Reson Med* **5,** 278–285.

[22] Bansal N and Seshan V (1995). Three-dimensional triple quantum-filtered ^{23}Na imaging of rabbit kidney with weighted signal averaging. *J Magn Reson Imaging* **5,** 761–767.

[23] Hall DE, Moffat BA, Stojanovska J, Johnson TD, Li Z, Hamstra DA, Rehemtulla A, Chenevert TL, Carter J, Pietronigro D, et al. (2004). Therapeutic efficacy of DTI-015 using diffusion magnetic resonance imaging as an early surrogate marker. *Clin Cancer Res* **10,** 7852–7859.

[24] Bansal N, Germann MJ, Seshan V, Shires GT, III, Malloy CR, and Sherry AD (1993). Thulium 1,4,7,10-tetraazacyclododecane-1,4,7,10-tetrakis(methylene phosphonate) as a ^{23}Na shift reagent for the *in vivo* rat liver. *Biochemistry* **32,** 5638–5643.

[25] Helmer KG, Meiler MR, Sotak CH, and Petruccelli JD (2003). Comparison of the return-to-the-origin probability and the apparent diffusion coefficient of water as indicators of necrosis in RIF-1 tumors. *Magn Reson Med* **49,** 468–478.

[26] Carano RA, Ross AL, Ross J, Williams SP, Koeppen H, Schwall RH, and van Bruggen N (2004). Quantification of tumor tissue populations by multispectral analysis. *Magn Reson Med* **51,** 542–551.

[27] Winter PM, Poptani H, and Bansal N (2001). Effects of chemotherapy by 1,3-bis(2-chloroethyl)-1-nitrosourea on single-quantum– and triple-quantum–filtered ^{23}Na and ^{31}P nuclear magnetic resonance of the subcutaneously implanted 9L glioma. *Cancer Res* **61,** 2002–2007.

[28] Makos JD, Malloy CR, and Sherry AD (1998). Distribution of TmDOTP 5^- in rat tissues: TmDOTP 5^- *vs* CoEDTA$^-$ as markers of extracellular tissue space. *J Appl Physiol* **85,** 1800–1805.

[29] Schwartz PS and Waxman DJ (2001). Cyclophosphamide induces caspase 9–dependent apoptosis in 9L tumor cells. *Mol Pharmacol* **60,** 1268–1279.

[30] Makin G (2002). Targeting apoptosis in cancer chemotherapy. *Expert Opin Ther Targets* **6,** 73–84.

[31] Duvvuri U, Poptani H, Feldman M, Nadal-Desbarats L, Gee MS, Lee WM, Reddy R, Leigh JS, and Glickson JD (2001). Quantitative T_1rho magnetic resonance imaging of RIF-1 tumors *in vivo*: detection of early response to cyclophosphamide therapy. *Cancer Res* **61,** 7747–7753.

[32] Rajan SS, Wehrle JP, Li SJ, Steen RG, and Glickson JD (1989). ^{31}P NMR spectroscopic study of bioenergetic changes in radiation-induced fibrosarcoma-1 after radiation therapy. *NMR Biomed* **2,** 165–171.

[33] Li SJ, Wehrle JP, Glickson JD, Kumar N, and Braunschweiger PG (1991). Tumor bioenergetics and blood flow in RIF-1 murine tumors treated with 5-fluorouracil. *Magn Reson Med* **22,** 47–56.

[34] Steen RG (1989). Response of solid tumors to chemotherapy monitored by *in vivo* ^{31}P nuclear magnetic resonance spectroscopy: a review. *Cancer Res* **49,** 4075–4085.

[35] Ben-Yoseph O and Ross BD (1994). Oxidation therapy: the use of a reactive oxygen species–generating enzyme system for tumour treatment. *Br J Cancer* **70,** 1131–1135.